



HAL
open science

Hydrometallurgical Processing of Chalcopyrite by Attrition-Aided Leaching

Amine Dakkoune, Florent Bourgeois, Adeline Po, Catherine Joulian, Agathe Hubau, Solène Touzé, Carine Julcour, Anne-Gwenaëlle Guezennec, Laurent Cassayre

► **To cite this version:**

Amine Dakkoune, Florent Bourgeois, Adeline Po, Catherine Joulian, Agathe Hubau, et al.. Hydrometallurgical Processing of Chalcopyrite by Attrition-Aided Leaching. ACS Engineering Au, 2023, 3 (3), pp.195-209. 10.1021/acsengineeringau.2c00051 . hal-04189254

HAL Id: hal-04189254

<https://cnrs.hal.science/hal-04189254v1>

Submitted on 28 Aug 2023

HAL is a multi-disciplinary open access archive for the deposit and dissemination of scientific research documents, whether they are published or not. The documents may come from teaching and research institutions in France or abroad, or from public or private research centers.

L'archive ouverte pluridisciplinaire **HAL**, est destinée au dépôt et à la diffusion de documents scientifiques de niveau recherche, publiés ou non, émanant des établissements d'enseignement et de recherche français ou étrangers, des laboratoires publics ou privés.



Distributed under a Creative Commons Attribution - NonCommercial - NoDerivatives 4.0
International License

Hydrometallurgical Processing of Chalcopyrite by Attrition-Aided Leaching

Amine Dakkoune, Florent Bourgeois, Adeline Po, Catherine Joulian, Agathe Hubau, Solène Touzé, Carine Julcour,* Anne-Gwénaëlle Guezennec, and Laurent Cassayre



Cite This: *ACS Eng. Au* 2023, 3, 195–209



Read Online

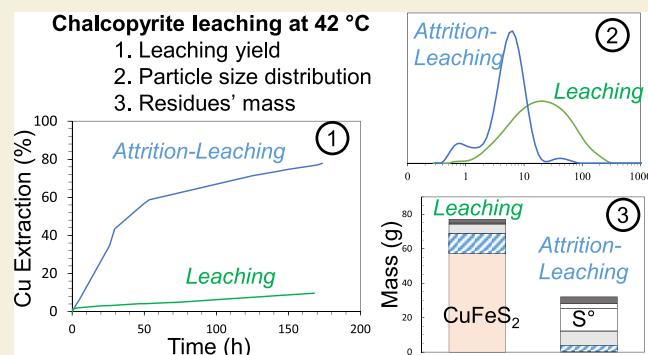
ACCESS |

Metrics & More

Article Recommendations

ABSTRACT: We report the investigation of a chalcopyrite leaching process that implements millimeter-sized glass beads that are stirred in the leach reactor to combine particle grinding, mechanical activation, and surface removal of reaction products. The paper focuses on demonstrating the impact of the so-called attrition-leaching phenomenon on the leaching rate of a chalcopyrite concentrate and provides a first understanding of the underlying mechanisms. For this purpose, we have compared the copper leaching yield for different configurations under controlled chemical conditions (1 kg of glass beads and 84 g of chalcopyrite concentrate in 2.5 L of $\text{H}_2\text{SO}_4\text{-H}_2\text{O}$ solution, pH = 1.3, $E_h = 700$ mV vs SHE, and $T = 42$ °C). On top of elemental analysis of the leach solution with time, we provide a full characterization of the solid residue based on X-ray diffraction, elemental analysis, and sulfur speciation. We demonstrate that glass beads led to a remarkable enhancement of the leaching rate in conditions where particles were already passivated by simple leaching and even when large amounts of solid products (elemental sulfur and jarosite) were present. An in-depth evaluation of particle size distribution showed that particle breakage occurred during a rather short time (a few hours) at the beginning of the runs, transforming the initial particles with $d_{4/3} = 30$ μm to finer particles with $d_{4/3} = 15$ μm . Then, particle breakage almost stopped, while an attrition phenomenon was evidenced, inducing the formation of very fine particles (<1 μm) and aggregates concomitantly with copper leaching.

KEYWORDS: hydrometallurgy, chalcopyrite sulfuric leaching, attrition-leaching, particle size, depassivation



1. INTRODUCTION

Manufacturing of metallic copper, whose worldwide demand is growing continuously, starts with copper mineral extraction, often found in Earth's crust as chalcopyrite (CuFeS_2) mineral,¹ which represents about 70% of the world's copper reserves.² Pyrometallurgical processes have been historically the main extraction way implemented by mineral industries, and smelting operations of copper concentrates are still dominant.³ However, the extraction of copper by hydrometallurgical routes has attracted special attention in the past 20 years, in the view of lower energy costs and environmental impacts,^{4,5} as well as to provide new options to process low grade ores, overburden, mining wastes, and urban mine wastes.⁶ Currently, more than 20% of copper produced in the world is extracted by hydrometallurgical processes, which requires an efficient dissolution operation before selective copper extraction. Leaching can be carried out at high pressure and high temperature with the addition of a leaching agent or at atmospheric pressure and moderate temperature by combination of an acid solution (generally sulfuric acid) and an oxidizing

agent such as oxygen, ferric ion, hydrogen peroxide, or manganese dioxide particles.^{5–8} As reviewed recently by Barton and Hiskey,⁹ alternative lixiviants (e.g., ionic liquids, glycine, and hypochlorites) are also investigated for this operation. Bioleaching has also been considered, but recent trends show that technological applications are scarce for copper sulfides.^{10,11}

Chalcopyrite leaching is very slow at moderate temperature, which is one of the main limiting factors in copper production in industrial conditions, but there is currently no consensus on the exact nature of the limiting step. Indeed, many authors (e.g., refs 12 and 13) base their explanation of dissolution inhibition on the formation of passivation layers around the solid particles of the mineral. The formation of different solid phases (e.g.,

Received: December 13, 2022

Revised: March 1, 2023

Accepted: March 2, 2023

Published: March 16, 2023



elemental sulfur,^{5,13,14} covellite (CuS) and chalcocite (Cu₂S),^{15–17} and jarosite^{18–20} have indeed been reported during chalcopyrite leaching. The formation of these solid phases could account for the reduction of the available and accessible surface of the mineral and thus severely limits the copper extraction efficiency.¹⁶ However, as discussed at length in the recent review of O'Connor and Eksteen,²¹ this common explanation is challenged by much experimental evidence. An alternative approach to the passivation model is linked to the electronic properties of chalcopyrite, which as a semiconductor exhibits a band gap that may hinder electron transfer and oxidation, especially since the energy range of this band gap coincides with the standard redox potential of common redox couples such as the ferric-ferrous couple.²¹ A recent experimental investigation from Ren et al.²² offers an explanation that combines the two phenomena. The proposed mechanism involves the formation of a covellite-like external layer due to preferential iron dissolution, with p-type electronic properties. This may produce a p–n junction on n-type bulk chalcopyrite that hinders further electrochemical processes. This complex and yet not fully elucidated mechanism, which results in well-documented slow dissolution of chalcopyrite concentrates in acidic oxidative media, will be referred to as “passivation” in the rest of the article.

To tackle the problem raised by leaching inhibition of chalcopyrite, numerous options have been investigated.^{5,7,23} For instance, chalcopyrite leaching may be operated at a temperature above the melting point of sulfur (115 °C) to disperse the solid sulfur or even at higher temperature (typically 220 °C) to oxidize it into soluble sulfate ions.²⁴ Although these options help to increase the reaction rate, they are expensive in terms of energy consumption; in addition, they require the deployment of pressurized reactors. Preliminary fine grinding of the ore (particle size of about 5–10 μm) to increase the exchange surface and dissolve maximum copper before passivation is another well-known option to enhance chalcopyrite leaching. A third alternative to enhance chalcopyrite leaching is mechanical activation, which consists in premilling the chalcopyrite concentrate in dedicated planetary mills using centimeter-sized balls.²⁵ For instance,^{26–29} various conditions of mechanochemical activation were investigated and all evidenced enhanced leaching of chalcopyrite, attributed to partial oxidation and rupture of the crystal lattice. Mechanistic studies from Bai et al.³⁰ and Li et al.³¹ confirmed that this enhanced leaching process combines grain size reduction and modification of crystal and lattice properties through the formation of defects. However, fine grinding of chalcopyrite and/or mechanical activation as pretreatment do not in any way prevent the effect of passivation of the particles within the leaching reactor.

In parallel, there are a few works that report an improvement of the leaching yield thanks to the direct addition of silica-based materials in the reactor. First, Misra and Fuerstenau³² showed that 50 nm silica particles (3–17 g·L⁻¹) increase the copper yield and called for further investigation of the associated mechanism. Dong et al.³³ also reported a noticeable improvement of copper bioleaching with 50 g·L⁻¹ fine quartz particles (<43 μm) in the leach solution. Jafari et al.³⁴ added 10–40 g·L⁻¹ silica particles (<200 μm) in the leaching reactor at 80 °C and observed a small improvement of leaching yield, together with a much cleaner grain surface at the microscopic scale. They concluded that the increase in copper yield was due to the combination of mechanical friction and collision that reduced the passive layers.

In the present paper, we report our investigations on a leaching reactor that aims to perform *in situ* mechanical abrasion of chalcopyrite's particle passivation layers. The objective is not to prevent their formation but to eliminate those that form on the surface of the particles so as not to impede or stop the leaching. This reactor implements millimeter-sized grinding glass beads that are stirred, promoting the abrasion of the ore particles by the application of surface stresses, rather than their impact fracturing, to continuously remove surface layers. The attrition-leaching concept was first tested and validated for mineral carbonation systems.^{35–38} It was demonstrated that it strongly reduces the passivation of silicate ores and nickel slag, with a dissolution yield after 24 h that goes from 5–10% to about 80%.^{37,39} Furthermore, a rather similar process is being implemented by FLSmidth to leach copper sulfide concentrates at 80 °C and under atmospheric pressure using interstage attrition/grinding to enhance the dissolution of copper-bearing minerals.⁴⁰ Due to the direct industrial application of this process (the so-called rapid oxidative leach process), not much fundamental work has been reported yet.

Based on these elements, we studied the impact of 1.2–1.6 mm glass beads at 400 g·L⁻¹ on the leaching of a chalcopyrite concentrate in a sulfuric acid solution. These conditions are thus different from previous studies^{32–34,41} implementing smaller (<200 μm) and lower quantities (<50 g·L⁻¹) of silica particles. According to the Pourbaix diagram for the CuFeS₂-H₂O system,⁴² to dissolve copper from chalcopyrite, a pH lower than 4 and a potential higher than 400 mV vs SHE are required. The experiments were thus carried out in a devoted leaching reactor at 42 °C, a pH of 1.3, and a potential of 700 mV vs SHE. These conditions, compatible with bioleaching, are favorable for complete dissolution of the CuFeS₂ phase from a thermodynamic point of view.⁴³ The main purpose of the work was to evaluate the effect of these millimeter-sized glass beads on the efficiency of chalcopyrite leaching and on the particle size evolution and to contribute to a better understanding of the passivation/depasivation mechanisms occurring on the surface of chalcopyrite particles.

2. MATERIALS AND METHODS

2.1. Chemicals and Materials

The copper concentrate was produced by flotation after extraction of the ore from Aitik mine (Sweden). It was sampled in 2019 and then homogenized and divided into multiple subsamples using riffle splitters. No specific precaution was taken during storage, which means that surface passivation by air most likely occurred.

The chemicals consisted of deionized water (0.05 μS·cm⁻¹), 95% sulfuric acid, and 30% hydrogen peroxide 30% solutions purchased from VWR INTERNATIONAL.

The glass beads (GlassBeads 1.5 type) were from Netzsch Group. The beads have a density of 2.5 kg·L⁻¹ and diameters that vary between 1.25 and 1.65 mm, with a chemical composition of 72.5 wt % SiO₂, 13 wt % Na₂O, 9 wt % CaO, and 4 wt % MgO.

2.2. Chemical and Structural Characterizations

Liquid samples from the leachate were analyzed by inductively coupled plasma–optical emission spectroscopy (ICP-OES) (PerkinElmer Optima 8300) for Fe and Cu quantification.

The characterization of the raw chalcopyrite concentrate and the leaching residues was carried out by complementary analytical techniques. Elemental analyses (systematically repeated on three samples) were performed by ALS Geochemistry (Galway, Ireland), by implementation of full mineralization followed by ICP-OES analysis of metal elements. The following analytical methods were implemented for sulfur analyses:

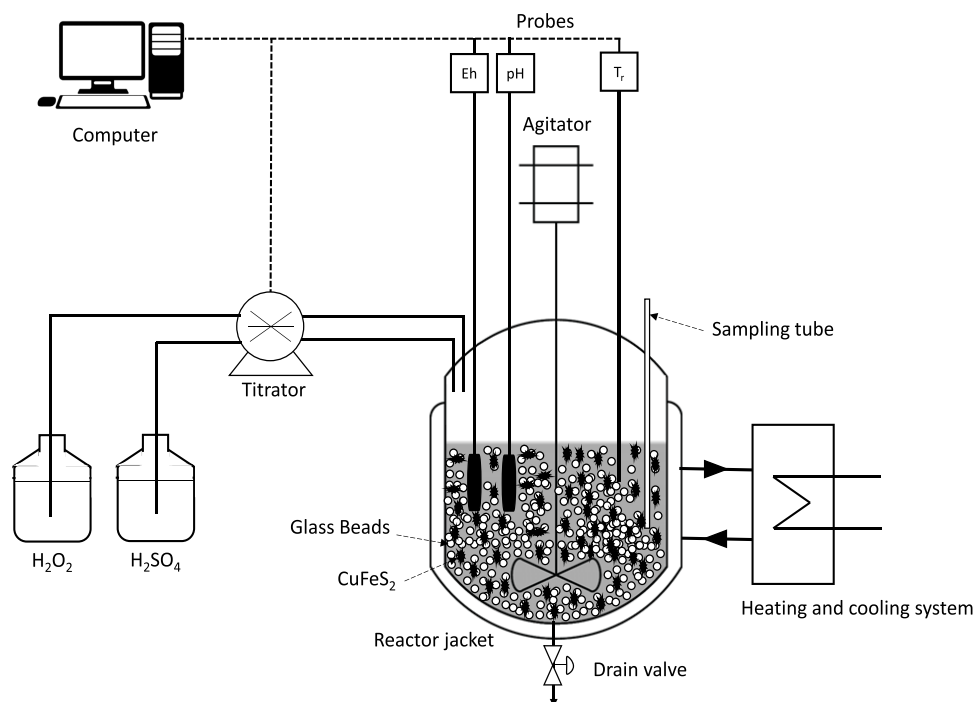


Figure 1. Schematic representation of the leach reactor.

- Elemental sulfur (S^0) was determined using a carbon disulfide leach. A portion of the leachate was evaporated to dryness, and the residue was weighed as elemental sulfur.
- S as sulfate (S_{SO_4}): a 1 g sample was treated with sodium carbonate to leach sulfates, filtered, then precipitated as barium sulfate, and analyzed gravimetrically.
- Sulfide ($S_{sulfide}$): A 0.1 g sample was leached with Na_2CO_3 , heated, and filtered via a Gooch crucible. The remainder was analyzed by an induction furnace and infrared spectroscopy to determine sulfide sulfur.

X-ray diffraction (XRD) was implemented with a D8 BRUKER in the $\theta/2\theta$ configuration and $Cu K\alpha$ radiation (2θ range of 20 – 80° with a wavelength of 1.5418 \AA). The samples were wet-micronized with ethanol, dried, and crumbled before being deposited on a support.

A scanning electron microscope-field emission gun (SEM-FEG, JEOL JSM 7100F) equipped with an EDX Oxford ASDD X-Max detector was used for particle observations (accelerating voltage, 10 kV ; working distance, 10 mm). Cross sections of the solid material were prepared by embedding the powders in a nonconducting thermosetting resin (PolyFast, STRUERS) for hot molding (Mecapress 3, PRESI) and diamond-polished down to $1 \mu\text{m}$ (Mecattech 234, PRESI).

Brunauer–Emmett–Teller (BET) analysis was carried out on an ASAP 2050 Micromeritics using nitrogen adsorption at 77 K . The density of the concentrate was determined by a helium gas pycnometer on an AccuPyc 1330 Micromeritics. For both measurements, the sample was degassed for a week at room temperature and weighed before analysis.

The particle size distribution (PSD) of raw chalcopyrite concentrate was obtained by laser diffraction in wet dispersion mode using a Malvern Mastersizer 3000. The index of refraction and absorption for the material were respectively 1.52 and 0.1 , and the stirring speed was fixed at 3500 rpm with five successive analyses carried out for each sample.

2.3. Leaching Reactor

A scheme of the experimental reactor is shown in Figure 1. It consisted of a glass jacketed reactor with a capacity of 6 L . The reactor was equipped with a four-blade Teflon stirrer attached to a variable speed motor (from 0 to 750 rpm). The circulation of water between the jacket

and a thermocryostat (AC200, Thermo Fisher) maintained the temperature at 42°C inside the reactor.

A PT100 platinum temperature probe (PT100 Duplex Probe, TC Direct), a combined pH electrode (LL-Unitrode SC, Metrohm), and a combined platinum annular electrode (Electrode Pt, Metrohm) with a $Ag/AgCl$ reference (3 M KCl) were immersed in the solution to measure the temperature, pH, and redox potential (E_h), respectively, throughout the duration of the experiment. Both electrodes were protected by a thin stainless-steel grid to prevent the probes from being damaged by the glass beads. pH and E_h were controlled by an automatic titrator (Titrand, Metrohm) using H_2SO_4 (95%) and H_2O_2 (30%), respectively.

The installation was linked to a computer that displayed and recorded the temperature. Acquisition and regulation of pH and E_h were carried out by Tiamo software.

2.4. General Experimental Protocol

Each experiment was started by adding 2.5 L of water and 84 g of the chalcopyrite concentrate in the reactor. The initial solid/(liquid + solid) ratio was thus equal to $3.25 \text{ wt } \%$ for all the runs (neglecting the small amounts of H_2SO_4 and H_2O_2 added to set constant pH and E_h). The glass bead amount was fixed to 1 kg , and the stirrer rotation speed was fixed to 556 rpm . Visual observation allowed one to ensure the complete suspension of chalcopyrite particles and beads during the run.

After reaching the target temperature ($42 \pm 1^\circ \text{C}$), the pH was adjusted and regulated to 1.3 ± 0.1 by the addition of H_2SO_4 . The solution potential was fixed and regulated to $700 \pm 10 \text{ mV}$ vs standard hydrogen electrode (SHE) by the addition of H_2O_2 . It can be noted that this potential was almost the highest potential that we could reach at pH = 1.3 using hydrogen peroxide, which is very consistent with recent measurements published in ref 44 in similar media. The conversion between the measured potential $E_{Ag/AgCl}$ (vs $Ag/AgCl$ in 3 M KCl) and E_{SHE} at 42°C was based on tabulated data from ref 45 according to eq 1:

$$E_{SHE} = E_{Ag/AgCl} + 194.6 \text{ (mV)} \quad (1)$$

During the runs and at periodic time intervals, 10 mL samples of the pulp were withdrawn by a syringe whose tip was inserted into a thin metal tube immersed in the reactor (Figure 1). The tube diameter was 0.8 mm , which prevented the collection of beads together with the slurry. About 8 mL of the samples was used for beads diffraction analysis,

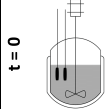
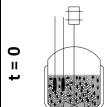
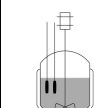
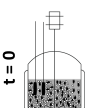
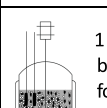
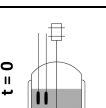
L Leaching		No beads for 170 h pH = 1.3 ; Eh = 700 mV vs SHE
AL Attrition-Leaching		1 kg of beads for 216 h pH = 1.3 ; Eh = 700 mV vs SHE
L-AL Leaching followed by Attrition-Leaching		No beads for 170 h pH = 1.3 ; Eh = 700 mV vs SHE
	Addition of beads	
		1 kg of beads for 100 h pH = 1.3 ; Eh = 700 mV vs SHE
A-L Attrition followed by Leaching		1 kg of beads for 3 h in water
	Removal of beads	
		No beads for 125 h pH = 1.3 ; Eh = 700 mV vs SHE

Figure 2. Summary of the experimental configurations.

Table 1. Elemental Composition and Phase Distribution (wt %) of the Raw Chalcopyrite Concentrate

elemental composition (wt %)															
ICP-OES									S speciation						
Fe	Cu	Si	Al	K	Na	Zn	Mo	Ca	S _{SO4}	S _{sulfide}	S ⁰				
30.60 ± 0.17	26.57 ± 0.23	2.90 ± 0.20	0.83 ± 0.05	0.37 ± 0.02	0.21 ± 0.02	0.25 ± 0.01	0.17 ± 0.01	0.13 ± 0.01	0.21 ± 0.01	33.27 ± 0.32	0.01 ± 0.01				
phase distribution (wt %)															
CuFeS ₂		FeS ₂		SiO ₂		MoS ₂		KAlSi ₃ O ₈		NaAlSi ₃ O ₈		Fe ₃ O ₄		total	
76.72		11.88		2.83		0.28		2.63		2.43		2.38		99.15	

while 2 mL was filtered through 0.2 μm syringe filters and analyzed by ICP-OES. The leaching yield $Y_{i(t)}^L$ of elemental species i at time t is expressed according to eq 2:

$$Y_{i(t)}^L(\%) = \frac{c_{m,i}(t) \cdot V_{\text{tot}}(t)}{m^0 \omega_i} \quad (2)$$

where $c_{m,i}(t)$ is the concentration of species i at time t in the leachate (g·L⁻¹), $V_{\text{tot}}(t)$ is the total volume of solution at time t (L), m^0 is the initial mass of chalcopyrite (g), and ω_i is the weight fraction of species i in the chalcopyrite concentrate. The total volume $V_{\text{tot}}(t)$ was derived from eq 3:

$$V_{\text{tot}}(t) = V_{\text{H}_2\text{O}} + V_{\text{H}_2\text{SO}_4}(t) + V_{\text{H}_2\text{O}_2}(t) - n(t) \cdot V_{\text{sample}} \quad (3)$$

with $V_{\text{H}_2\text{O}}$ being the volume of water added at the beginning of leaching (L), $V_{\text{H}_2\text{SO}_4}$ being the volume of sulfuric acid added in solution (L), $V_{\text{H}_2\text{O}_2}$ being the volume of hydrogen peroxide added in solution (L), V_{sample} being the volume of slurry sampled (L), and n being the number of samples.

At the end of the run, the whole reactor content was drained and first separated from the beads on a stainless steel sieve (RETSCH) with a mesh size of 850 μm. Then, the beads were washed several times with deionized water to recover the remaining suspension that was stuck on the beads. The beads were then dried in an oven at 100 °C for 24 h and weighed. They were reused in the next experiment. The resulting suspension was centrifuged (SIGMA Laboratory Centrifuges) at a speed of 11,000 rpm during 5 min to get rid of the liquid phase. Then, the wet solid was dried in an oven (Thermo Electron Corporation) at 100 °C for 24 h. The dried solid was finally weighed, crushed, mixed, and quartered for analyses. The copper leaching yield Y_{Cu}^S obtained from the solid residue was calculated according to eq 4.

$$Y_{\text{Cu}}^S(\%) = 100 \left(1 - \frac{m^{\text{res}} \omega_{\text{Cu}}^{\text{res}}}{m^0 \omega_{\text{Cu}}^0} \right) \quad (4)$$

where m^{res} and m^0 are the mass of the initial sample (84 g) and of the solid residue, and $\omega_{\text{Cu}}^{\text{res}}$ and ω_{Cu}^0 are the mass fraction of Cu in the chalcopyrite concentrate and in the solid residue, respectively.

2.5. Run Configurations

Four operating procedures were carried out, defined according to the presence of the glass beads in the reactor. The conditions of these four configurations are as follows (see also Figure 2):

- Leaching test (L) is a leaching-only test (without glass beads).
- Attrition-leaching test (AL) combines leaching and attrition throughout the entire test. Glass beads are therefore present in the reactor throughout the test.
- Leaching followed by attrition-leaching (L-AL) is a leaching test followed by an attrition-leaching test. Glass beads are introduced in the reactor after the pulp has been subjected to a preliminary leaching test.
- Attrition followed by leaching (A-L): The chalcopyrite concentrate is pretreated in 2.5 L of pure water in the presence of 1 kg of beads without pH or E_h regulation (and in particular, no addition of acid). After 3 h, the pulp is separated from the grinding beads on a stainless steel sieve. Note that the ICP-OES analysis of the aqueous phase has shown negligible dissolution of copper and iron at this stage. Then, the pulp is put back in the reactor and pH and E_h are adjusted to their set values.

All process parameters were similar in each configuration: 84 g of chalcopyrite concentrate, 2.5 L of water, 1 kg of glass beads (when present), T set at 42 °C, pH regulated at 1.3, E_h regulated at 700 mV vs SHE, stirring speed of 556 rpm, and duration of about 125 h.

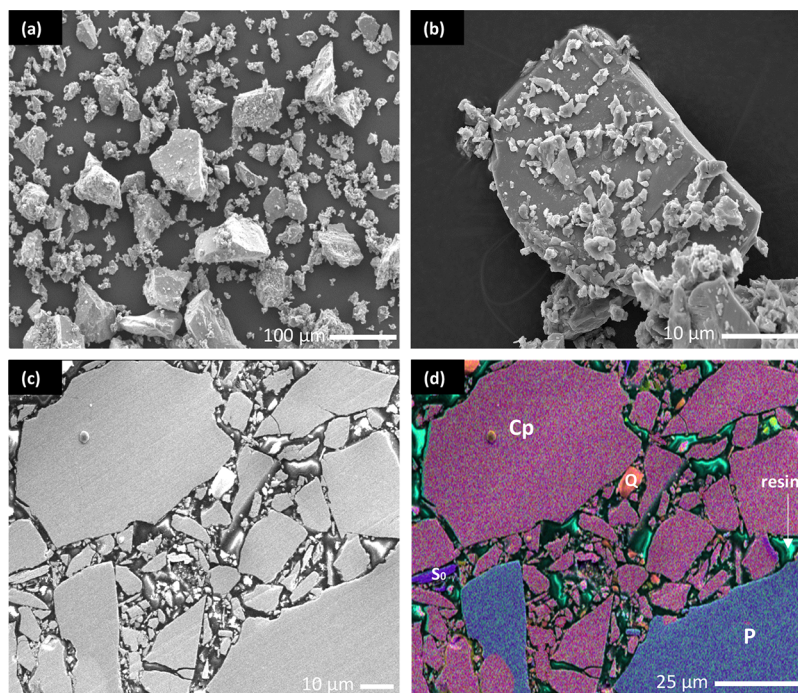


Figure 3. SEM images of raw chalcopyrite concentrate: (a, b) direct observation of the powder; (c, d) observation and EDX mapping of a cross section of an embedded sample. Cp: chalcopyrite; P: pyrite; Q: quartz; S₀: elemental sulfur.

3. RESULTS AND DISCUSSION

3.1. Raw Concentrate Characterization

The XRD phase identification of the raw concentrate, presented in Figure 7, shows the presence of two major phases (chalcopyrite (CuFeS₂) and pyrite (FeS₂)) and two minor phases (quartz (SiO₂) and molybdenite (MoS₂)). Additionally, peaks of weak intensity could be attributed to microcline (KAlSi₃O₈), albite (NaAlSi₃O₈), and magnetite (Fe₃O₄).

The average chemical composition of the raw chalcopyrite concentrate, determined by ICP-OES and sulfur speciation on three samples, is compiled in Table 1. The analyses show that the concentrate contains a total of 86.7 wt % of Cu, Fe, and S_{sulfide}, with minor amounts of Si, Al, Mo, K, Na, Zn, Ca, S_{SO₄}, and S₀. Based on XRD and elemental analyses, the composition of the chalcopyrite concentrate has been established according to the following hypotheses: (i) Cu is only in CuFeS₂, (ii) Mo is only in MoS₂, (iii) S_{sulfide} is only in CuFeS₂, MoS₂, and FeS₂, (iv) K is only in KAlSi₃O₈, (v) Na is only in NaAlSi₃O₈, (vi) remaining Fe is in Fe₃O₄, and (vii) remaining Si is in SiO₂.

As a result, the repartition of the main phases in the concentrate comes to 76.7 wt % of chalcopyrite and 11.9 wt % of pyrite (FeS₂), with other phases specified in Table 1. The total phase distribution accounts for 99.15% of the mass, which indicates that no significant phase is missing.

SEM images of the powder shown in Figure 3a,b reveal the presence of large (10–100 μm) particles, with smaller grains (~1 μm) deposited on their surface. The chemical analysis of cross sections of the chalcopyrite concentrate in Figure 3c,d confirms the presence of the major phases, namely, chalcopyrite CuFeS₂ (in pink), pyrite FeS₂ (in blue), and quartz SiO₂ (in orange), with a high degree of release.

The BET surface area of the raw chalcopyrite concentrate is 0.31 m²·g⁻¹, which reflects a nonporous microstructure, and its structural density equals 4.02 g·cm⁻³. Figure 4 shows the corresponding PSD in volume. As a dry powder, the volume

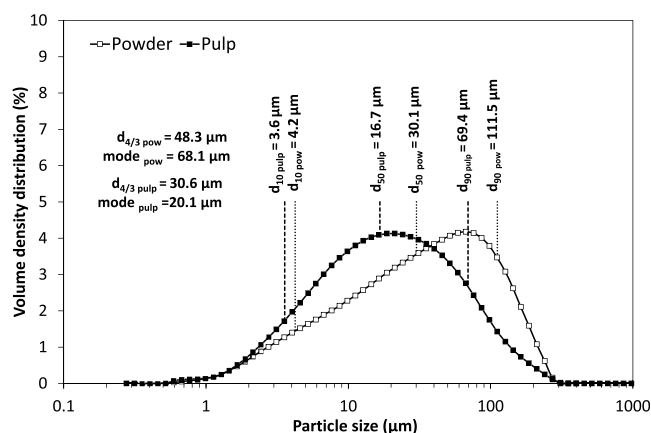


Figure 4. PSD (in volume) of the raw chalcopyrite concentrate as dry powder and as pulp after dispersion in water for 2 h with a stirring rate of 556 rpm.

mean diameter ($d_{4/3}$) value is 48.3 μm, with a main mode at 68.1 μm. When dispersed in water for 2 h with a stirring rate of 556 rpm, the powder size distribution is noticeably shifted toward finer particles, most likely due to deagglomeration. This second distribution, with $d_{4/3}$ = 30.6 μm and a main mode at 20.1 μm, is taken as a reference for comparison with PSD measured on samples collected during the runs.

3.2. Effect of Glass Beads on Cu and Fe Leaching Rate

Figure 5 compiles the evolution of copper yield Y_{Cu}^L (Figure 5a) and iron yield Y_{Fe}^L (Figure 5b) as a function of time for the four configurations.

A low yield of copper and iron (Figure 5, black squares) was the characteristic feature of simple leaching (L): after 168 h, about 9.6% of copper and 9.8% of iron were leached. The test was repeated twice and led to very similar yields. As discussed in the introduction of this paper, such low dissolution yield is well

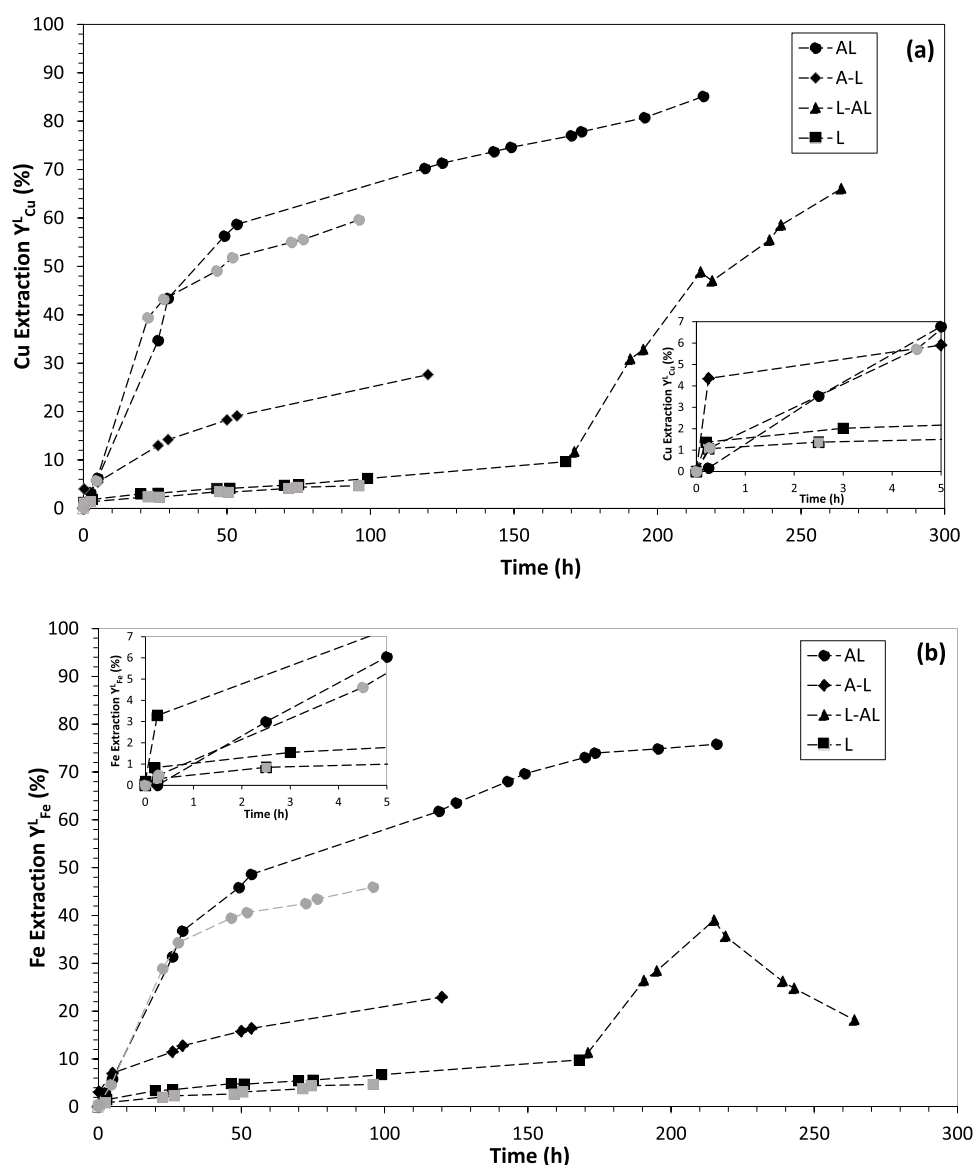


Figure 5. Copper (a) and iron (b) extraction yields during the various runs operated with 84 g of chalcopyrite concentrate, 2.5 L of water, 1 kg of glass beads (when present), $T = 42\text{ }^{\circ}\text{C}$, $\text{pH} = 1.3$, $E_h = 700\text{ mV}$ vs SHE, and a stirring speed of 556 rpm (leaching (L), attrition-leaching (AL), leaching followed by attrition-leaching (L-AL), and attrition followed by leaching (A-L)). Gray symbols correspond to 96 h duplicates of L and AL configurations.

described in the literature. A similar copper extraction yield (around 10%) was for instance reported in the work of Dong et al.³³ under conditions very close to this work (170 h, pH of 1.0 in H_2SO_4 leach media, $T = 42\text{ }^{\circ}\text{C}$, and $E_h = 750\text{ mV}$ vs SHE adjusted and controlled by H_2O_2 solution), except for the solid/(liquid + solid) ratio that was roughly 10 times lower (0.3% vs 3.2% in the present work). These authors also showed that, in these conditions, the copper yield reached 80% after about 300 h and that leaching was strongly activated at higher temperature (65–75 $^{\circ}\text{C}$). Khoshkhou et al.¹⁴ obtained 50% copper recovery after 144 h only ($\text{pH} = 1.4$ and $E_h = 710\text{ mV}$ vs SHE), but the temperature was much higher ($T = 80\text{ }^{\circ}\text{C}$). It is interesting to note that these authors compared the behavior of freshly ground and aged (2 years) chalcopyrite concentrates and showed that the freshly ground concentrate exhibited a much faster dissolution, most probably due to the formation of passivation layers on the aged chalcopyrite particles due to air oxidation. As mentioned in Section 2, our chalcopyrite concentrate is

considered aged since it was stored for several months without specific precautions against oxidation (no use of inert gas or a close container).

The presence of 1 kg of glass beads (attrition-leaching AL, black circles in Figure 5) had a strong effect on the reaction kinetics and extraction performance, with an initial leaching rate increased by 14.5-fold and final yields reaching 85.1% for copper and 75.8% for iron after 216 h. The remarkable effect of the glass beads, which occurs mainly during the first 40–50 h, might be attributed to the exfoliation of the passivation layers formed on particles (the so-called attrition effect) but also to the increase in the specific surface of the particles due to their grinding. Indeed, it has been long established that the smaller the particle size, the faster the leaching rate.⁴⁶ The two other experimental configurations provide more insight on these aspects.

First, in the A-L configuration where the aqueous slurry was first agitated during 3 h in the presence of glass beads before acid addition (Figure 2), the copper and iron leaching yields were

enhanced compared to simple leaching (black diamonds in Figure 5). For instance, at $t = 120$ h, the leaching yields increased from 8 to 30% for copper and from 8 to 23% for iron. This is attributed to the grinding effect of the beads. Furthermore, at the very first beginning of the run (see the inset in Figure 5), the A-L configuration was also more efficient than the reference attrition-leaching test. Again, the grinding effect of the beads might be responsible for the enhanced initial leaching rates. However, after about 5 h, both copper and iron yields were higher when leaching was performed in the presence of beads, which illustrates the efficiency of attrition for the constant removal of passivation layers that inhibit the dissolution. This discussion will be completed in Section 3.4 on the basis of particle size analysis.

Second, the addition of beads after simple leaching in the L-AL configuration strongly activated the leaching of iron and copper (Figure 5, black triangles). Indeed, the yield of copper reached 34% after 24 h and 72% after 96 h. Again, this could be attributed to the combined effect of grinding and attrition, which both generate a fresh chalcopyrite surface. It can also be noted that, in this specific run, the yield of iron reached 40.5% after 48 h but was followed by a noticeable decrease up to 18.8% at the end of the run. This was attributed to the precipitation of a Fe-bearing solid that will be further discussed in Section 3.3.

Duplicates of the L and AL configurations were carried out for 96 h (gray symbols in Figure 5). Despite some differences in the dissolution yields, these duplicates confirm the overall role of the beads on the leaching rate of the concentrate.

As illustrated in Figure 6, the plot of the evolution of the concentrations (in $\text{mol}\cdot\text{L}^{-1}$) of Fe versus Cu in the aqueous phase shows a rather linear trend for all the tests, which is the sign of a similar dissolution mechanism for each run configuration, apart from the partial precipitation of iron occurring in the L-AL configuration (black triangles). Furthermore, the dissolution of iron was systematically greater

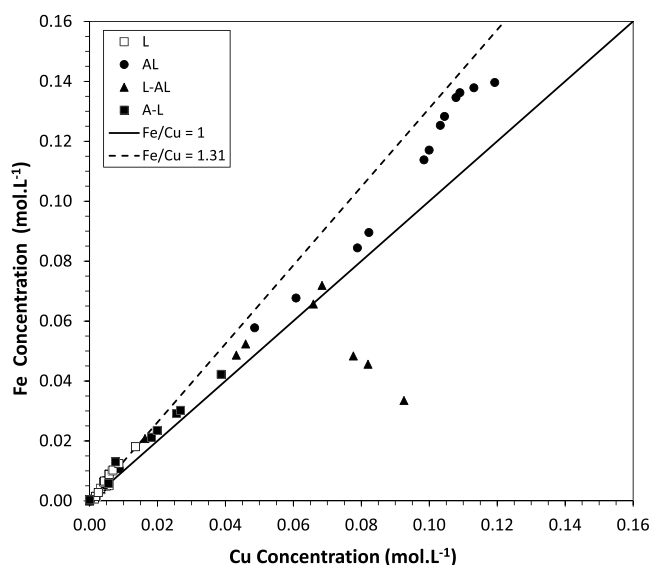


Figure 6. Evolution of iron concentration versus copper concentration in the aqueous phase during experiments at $T = 42$ °C, $\text{pH} = 1.3$, and $E_h = 700$ mV vs SHE (leaching (L), attrition-leaching (AL), leaching followed by attrition-leaching (L-AL), and attrition followed by leaching (A-L)); comparison to the Fe/Cu molar ratio of pure chalcopyrite (Fe/Cu = 1.0) and the chalcopyrite concentrate (Fe/Cu = 1.31).

than that of copper, which can be attributed to the codissolution of chalcopyrite and pyrite, the last mineral accounting for 11.9 wt % of the initial concentrate (Table 1). More precisely, our data show that the dissolution of chalcopyrite (Fe/Cu = 1) is faster than that of pyrite (no Cu), since the Fe/Cu molar ratio in the leachate was lower than the overall Fe/Cu molar ratio of the initial concentrate (Fe/Cu = 1.31). This behavior is in agreement with the current understanding of galvanic interactions between metal sulfides. Indeed, as illustrated for instance by the measurements and literature review of Tanne and Schippers,⁴⁷ the chalcopyrite rest potential is significantly lower than that of pyrite, and thus, chalcopyrite leaches preferentially than pyrite in the case of electrical contact between the two minerals. However, it has also been recently shown that, if the galvanic coupling can strongly enhance the chalcopyrite leaching rate at high temperature (e.g., at 80 °C in the Galvanox process⁴⁸), this effect is only marginal at moderate (20–30 °C) temperature.^{47,49} As a consequence, it is very likely that the relatively high content of pyrite (12 wt %) in our concentrate did not induce a significant effect on chalcopyrite dissolution rate in our tests.

The characterization of the solid residues, presented in the following section, provides more insight on the nature of the reactions occurring during leaching.

3.3. Characterization of the Solid Residues

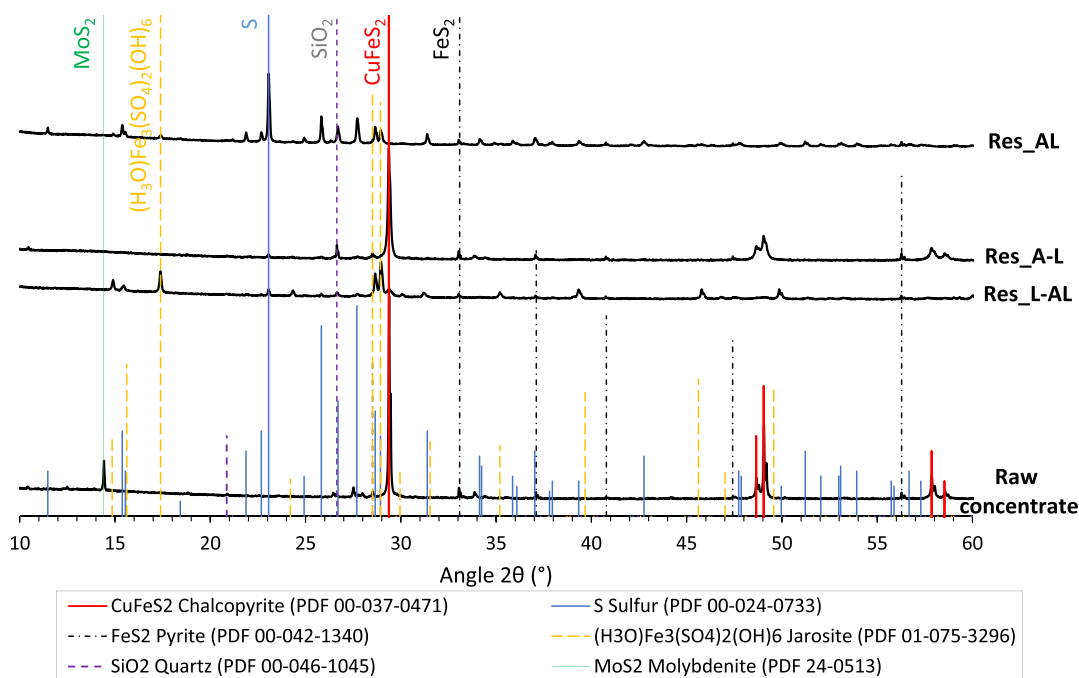
Following the various leaching tests, the solid residues consisting of undissolved chalcopyrite concentrate, solid reaction products, and any fragmented pieces of glass beads were recovered, washed, and dried for XRD and elemental analyses, as well as electron microscope observations (Section 2.2). Some properties of the residues are compiled in Table 2. Specifically, the copper leaching yield Y_{Cu}^{S} obtained from the solid residue (eq 4) is compared to the copper leaching yield Y_{Cu}^{L} obtained from solution analysis (eq 2). It comes from this comparison that Y_{Cu}^{S} is significantly higher than Y_{Cu}^{L} . We have no definitive explanation for this discrepancy, which could be due to errors in the assessment of the total mass of liquid or solid phase. However, both copper yields reflect the same tendency between test configurations; thus, qualitative discussion remains possible, especially in the frame of the present work focused on the impact of attrition induced by glass beads on the overall leaching process.

3.3.1. Phase Identification. The diffractogram of the residues Res_L obtained from the leaching tests L (not shown here) was similar to that of the raw concentrate (Figure 7), which is consistent with the very low leaching yield. The powder diffractograms of the solid residues obtained in the three configurations involving the glass beads are shown in Figure 7, together with phase identification.

The signal of the chalcopyrite phase appeared as follows in the diffractograms of the solid residues: a peak with strong intensity for Res_A-L, a weak signal for Res_L-AL, and no signal at all for Res_AL. These observations are in accordance with the final Cu leaching yields (Table 2) and confirm the strong influence of the configuration on chalcopyrite dissolution. This influence is not as strong on the pyrite phase, which is detected at rather similar intensity in the three diffractograms. This is consistent with the analysis of Fe/Cu ratio in the solution (Figure 6) and confirms that chalcopyrite leaches preferentially toward pyrite as discussed in Section 3.2. Finally, quartz is present in the three residues, with a significantly lower signal for the Res_L-AL test that is not explained at this stage.

Table 2. Properties of the Four Solid Residues

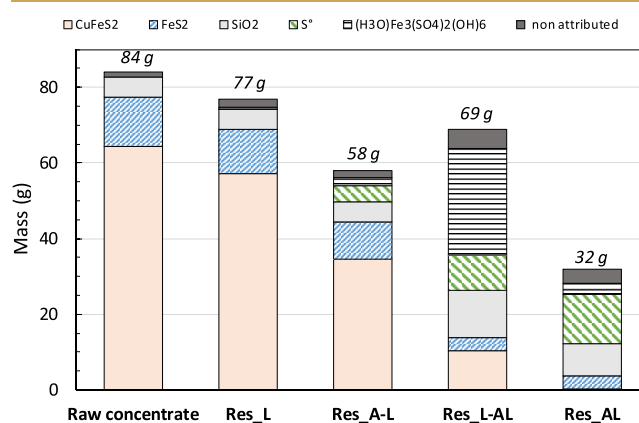
sample reference	test configuration	time in reactor (h)	Cu leaching yield from solution analysis Y_{Cu}^L (%)	Cu leaching yield from solid analysis Y_{Cu}^S (%)	dry mass m^{res} (g)
Res_L	leaching (L)	96	4.7	11.4	77
Res_AL	attrition-leaching (AL)	216	85.1	99.6	32
Res_L-AL	leaching followed by attrition-leaching (L-AL)	264	68.0	84.0	69
Res_A-L	attrition followed by leaching (A-L)	120	27.6	46.2	58

**Figure 7.** Powder XRD analysis of raw chalcopyrite concentrate and solid residues after attrition-leaching (AL), leaching followed by attrition-leaching (L-AL), and attrition followed by leaching (A-L) runs.

As for the main reaction products, phase identification showed a significant presence of elemental sulfur and hydronium jarosite $(H_3O)Fe_3(SO_4)_2(OH)_6$ (Figure 7), essentially for Res_AL and Res_L-AL, associated with high copper yields. A major feature is that the sulfur peaks are very intense in the AL configuration, while jarosite represents the dominant peak in the residue issued from the L-AL test. It can also be pointed out that the presence of jarosite in Res_L-AL is consistent with the decrease in iron content in the solution evidenced by elemental analysis (Figure 5b).

3.3.2. Elemental Analyses and Phase Speciation. Based on the elemental analysis of the residues, including sulfur speciation (see Section 2.2), and assuming that the main phases were identified by XRD (Figure 7), we calculated the phase distribution according to the following hypotheses: (i) all copper was in $CuFeS_2$, (ii) all $S_{sulfate}$ was in jarosite $(H_3O)Fe_3(SO_4)_2(OH)_6$, (iii) the remaining iron was in FeS_2 , (iv) all S° was in elemental sulfur, and (v) all Si was in SiO_2 . For the sake of simplicity, minor elements present in the raw concentrate (Mo, Al, Na, and K; see Table 1) were not taken into account in this overall estimation. We also recalculated a simplified composition of the raw concentrate based on hypotheses (i), (iii), and (v) for the purpose of comparison with the residues. Then, we calculated the mass of each phase in each solid sample by combining the mass of residue (Table 2) and the phase distribution.

The phase distributions derived from these calculations are presented in Figure 8 for all the residues, as well as the raw concentrate. Consistent with XRD analyses, chalcopyrite is the dominant phase in the residues obtained from the two configurations, leading to low copper dissolution yields. The quantity of pyrite in these two residues only slightly decreased compared to the raw concentrate, confirming the preferential dissolution of chalcopyrite vs pyrite, as evidenced from solution

**Figure 8.** Quantification of the main phases contained in the raw concentrate and in the solid residues, derived from elemental analyses and sulfur speciation.

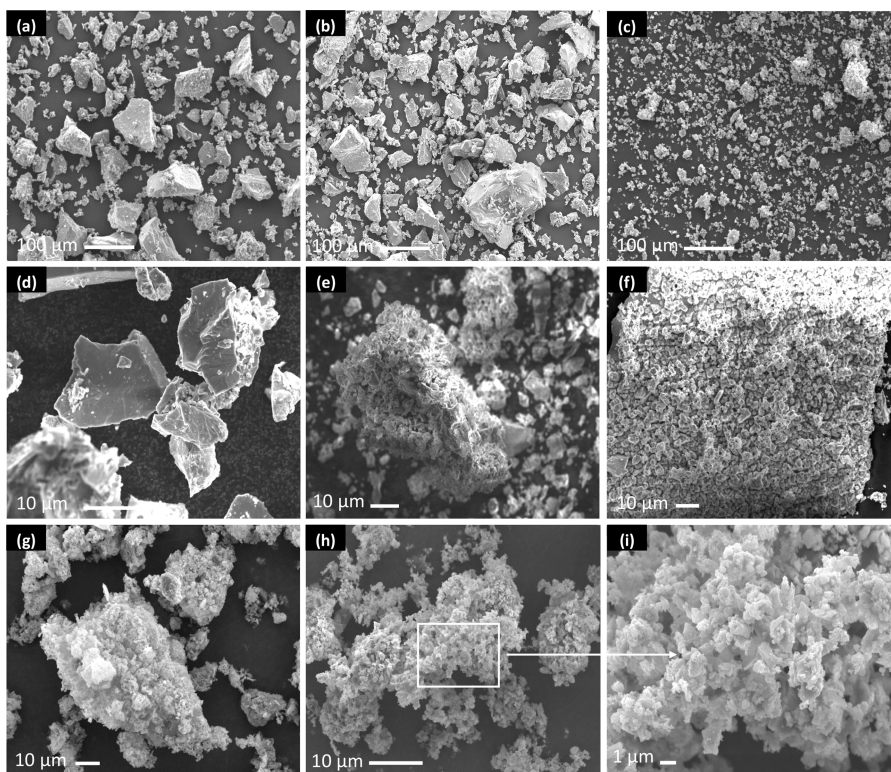
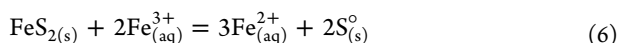
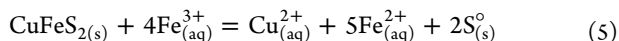


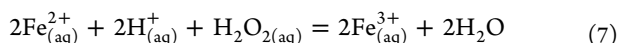
Figure 9. SEM micrographs of (a) raw chalcopyrite concentrate and solid residues obtained after (b) 168 h of leaching test L (no beads) and after 10 min (d), 2 h (e), 5 h (f), and 168 h (c, g–i) of attrition-leaching test AL (1 kg of beads) at pH = 1.3, $E_h = 700$ mV vs SHE, and $T = 42$ °C.

analysis (Figure 6). As for the residues obtained from the two tests carried out with glass beads (Res_AL and Res_L-AL), the overall quantities of chalcopyrite and pyrite in the residue were less than 10 and 5 g, respectively, which are consistent with the high leaching yields. Less than 1 wt % of the initial copper remained in the Res_AL residue, resulting in a copper leaching yield of 99% based on the solid phase. As highlighted at the beginning of this section, there is a noticeable discrepancy between the copper leaching yields obtained from solution analysis and solid analyses (Table 2).

The most generally accepted reactions during leaching involve the $\text{Fe}_{(\text{aq})}^{3+}$ aqueous species as the oxidant for both chalcopyrite and pyrite phases:^{5,7,12}



In our experimental conditions, no $\text{Fe}_{(\text{aq})}^{3+}$ was present at the beginning of the runs; it is thus likely that oxidative leaching was initiated by the presence of hydrogen peroxide. Then, as proposed for instance by Li et al.,^{50,51} the additions of hydrogen peroxide generated by E_h regulation led to $\text{Fe}_{(\text{aq})}^{3+}$ formation according to:



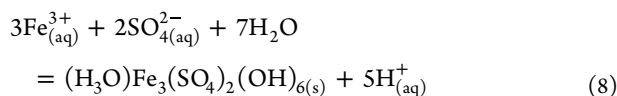
The occurrence of this reaction was clearly evidenced by Ma and Lin,⁵² who showed that the injection of H_{2}O_{2} into a $\text{H}_{2}\text{SO}_{4}$ - FeSO_{4} - H_{2}O solution in very close conditions (pH = 2, $\text{Fe}^{2+} = 55$ mg·L⁻¹, and $T = 30$ °C) to those of our work caused a sudden decrease in Fe^{2+} within the first 5 min of the experiment. In our runs, a substantial amount of hydrogen peroxide solution was added (e.g., about 155 mL in run AL, corresponding to 1.5 mol

of H_{2}O_{2}), and thus, we believe that the chalcopyrite and pyrite leaching occurred according to eqs 5 and 6, combined with regeneration of $\text{Fe}_{(\text{aq})}^{3+}$ by eq 7.

It can also be mentioned that, with the objective of establishing whether the presence of bacterial development could have occurred during the runs, microbial DNA extraction was performed on pulp samples taken at the end of an AL experiment. The DNA extraction procedure has been described in ref 53 and is adapted for the recovery of microbial DNA from bioleaching pulp samples. Fluorometric detection in the DNA extracts and attempts to amplify the 16S rRNA gene (a universal marker present in all bacteria) of the DNA extracts by polymerase chain reaction were both negative. These results established the absence of bacterial development during the experiments and ruled out the possibility to attribute chemical reactions (e.g., elemental sulfur or ferrous ion oxidation) to bacterial activity.

As evidenced by XRD analyses, large amounts of solid products were generated during AL and L-AL tests. An important conclusion is that these reaction products did not hinder the leaching, most likely in relation to the action of glass beads. Indeed, elemental sulfur and jarosite represented jointly roughly 50 wt % of the mass of the residues. Res_AL contained a large proportion of elemental sulfur (13 g) with some jarosite (3 g), while in the case of Res_L-AL, there was a much higher content of jarosite (28 g) and much less sulfur (9 g).

The massive precipitation of jarosite in the L-AL test could be attributed to a high sulfate content in the solution due to the addition of $\text{H}_{2}\text{SO}_{4}$ to maintain pH. Indeed, the solubility product of jarosite, as described by eq 8, is dependent on both $\text{Fe}_{(\text{aq})}^{3+}$ and $\text{SO}_{4(\text{aq})}^{2-}$ concentrations:



However, the amount of acid consumed in AL and L-AL configurations at the time of jarosite precipitation is lower in the L-AL test than in the AL test (29.1 mL of acid versus 56.0 mL, respectively), and the $\text{Fe}_{(\text{aq})}^{3+}$ concentration is also lower in the L-AL test (Figure 5b). Last, it comes from the quantification of the Si element in the residue that a small amount of glass bead fragments was incorporated in Res_L-AL and Res_AL (Figure 8), since their SiO_2 content was 8–12 g, while the initial SiO_2 content of the chalcopryrite concentrate was about 5 g only. Compared to the total mass of beads present in the leaching reactor (1000 g), it means that less than 1 wt % of the beads was crushed into small particles and incorporated in the residues. The highest amount of SiO_2 was found in Res_AL, where it represented about 25 wt % of the residue.

3.3.3. Electron Microscope Observations. Some SEM micrographs of solid residues are shown in Figure 9. They point out that almost no change occurred in the morphology of particles recovered after the leaching test L (Figure 9b) compared to the initial chalcopryrite concentrate (Figure 9a), in accordance with the low leaching yield. Nevertheless, the edges of large particles seem less sharp after the leaching test. This slight wear can be attributed to partial leaching or autogenous attrition.

On the other hand, the particles recovered from the attrition-leaching test are much smaller ($<10 \mu\text{m}$) (Figure 9c), with very different facies. Indeed, while the surface of the raw concentrate particles is rather smooth, the particles resulting from attrition-leaching exhibit a dendritic structure, which possibly results from smaller particle agglomeration or crystal growth. Although this concerns quite different conditions, a similar mechanism of aggregate formation during attrition-leaching of nickel slags has been recently demonstrated by Dufourny et al.⁵⁴

3.4. Effect of Glass Beads on Particle Size

PSD was measured by the laser diffraction analysis of various samples collected during the tests.

A preliminary investigation was carried out by introducing the chalcopryrite concentrate in the reactor filled with water and glass beads (without acid) and stirring at 556 rpm for 3 h (similar conditions to the preparation of the A-L test; see Figure 2). Elemental analysis of the solution after 3 h indicated that no significant dissolution of Cu or Fe took place during this operation. The evolution of the PSD is shown in Figure 10. The breakage effect from the beads is significant, with a progressive shift toward small particle sizes showing a main mode of about $4 \mu\text{m}$ after 3 h versus $20 \mu\text{m}$ initially.

Figure 11 compiles volume size distribution data obtained in the four test configurations. Each configuration provided some insights into the effect of the glass beads on the leaching process. The leaching test L (Figure 11a) exhibited almost no change in size distribution with respect to the initial chalcopryrite particles over the duration of the test (168 h). This is consistent with a slow surface dissolution process, leading to a low leaching yield (Figure 5) and overall mass loss (Table 2), as well as the great similarity of the particles observed by SEM compared to the initial concentrate (Figure 9).

With the A-L experiment (Figure 11b), the initial attrition step led to significantly finer initial particles with $d_{90} = 19.5 \mu\text{m}$, as already discussed (Figure 10). After removal of the beads (which corresponds to $t = 0$ in Figure 11b), the PSD remained

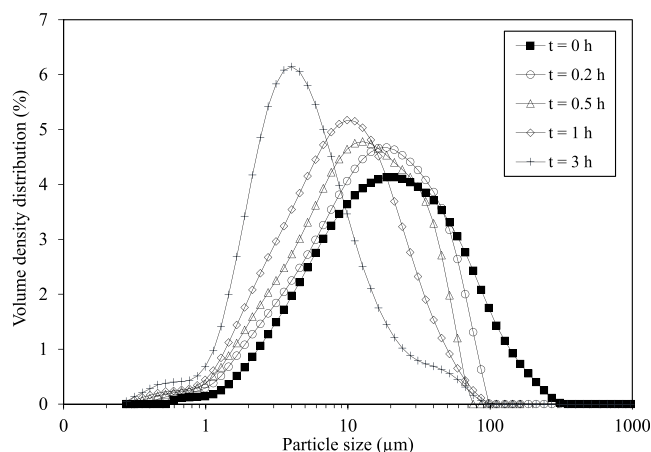


Figure 10. Volume size distribution of particles sampled from the reactor during a short test carried out in water only with 1 kg of glass beads.

rather constant. We attribute the slight shift of particles toward larger sizes to the partial aggregation of some fine particles and possibly the growth of element sulfur on the surface of the particles.

In the presence of beads (Figure 11c,d, corresponding to AL and L-AL configurations), the first observation is that the long-term attrition conditions did not lead to a very fine grinding of the particles, since a noticeable part of the distribution corresponds to particles with a size of about $10 \mu\text{m}$. The test also produced submicronic fines, whose proportion increased over time. The interpretation of these PSDs is not straightforward, and since three distinct modes were recurrently observed, it was decided to deconvolute the measured PSD using a mixture of 3 lognormal distributions $f_i(x)$ with parameters (μ_i, σ_i) , according to eq 9:

$$f(x) = \sum_{i=1}^3 \lambda_i f_i(x) \text{ and } x = \text{Lognormal}(\mu_i, \sigma_i) \quad (9)$$

where λ_i is the proportion of the i -th lognormal distribution.

The deconvolution was carried out by a least-squares fit of the measured cumulative PSD for both volume and surface area distributions (the surface area distribution is deemed important in such a process given that both leaching and attrition are surface-driven processes). A typical deconvolution example is provided in Figure 12. All data were analyzed in the same way, apart from the samples issued from the simple leaching experiments for which only one single mode was observed.

Figure 13 shows the values of the three modes (in μm) and their relative proportions (in %) as obtained from the deconvolution of the volume (Figure 13a) and surface area (Figure 13b) PSD for all available samples of the three tests (AL, L-AL, and A-L) and the reference sample (Figure 4). This compilation shows that, irrespective of sampling time or test configuration, the slurry is invariably composed of a mixture of very fine particles (less than $1 \mu\text{m}$), medium-sized particles (between 4 and $9 \mu\text{m}$ in volume and between 3 and $7 \mu\text{m}$ in surface), and larger particles (between 20 and $65 \mu\text{m}$ in volume and between 15 and $45 \mu\text{m}$ in surface). Thereafter, these modes are referred to as mode 1 (fine particles), mode 2 (medium), and mode 3 (large). Since the three tests did not lead to similar leaching yields, and since the resulting PSD was very different with and without beads, we conclude that, between attrition and

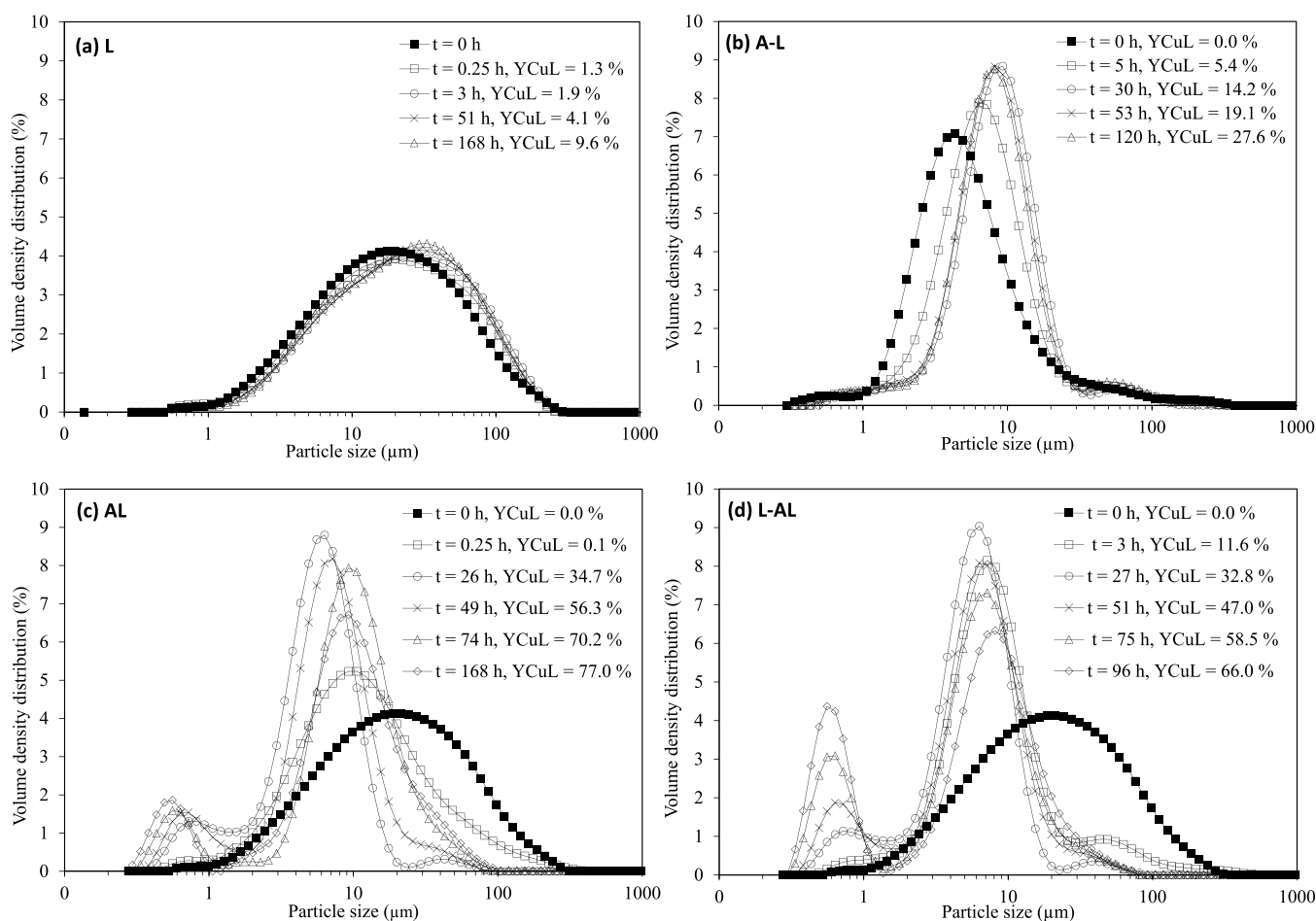


Figure 11. Volume size distribution of particles sampled from the reactor at different times in the four configurations: (a) leaching (L), (b) attrition followed by leaching (A-L), (c) attrition-leaching (AL), and (d) leaching followed by attrition-leaching (L-AL).

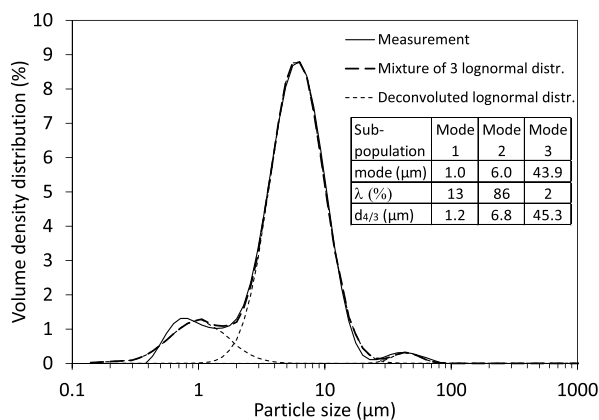


Figure 12. Example of volume PSD signal deconvolution with corresponding distribution parameters (configuration AL at $t = 26$ h).

dissolution, it is attrition that determines particle size in our process.

Further analysis of the data was carried out by plotting the evolution of the proportion of the three populations of particles, on a volume and surface area basis, as a function of time (Figure 14). The leaching rate, evaluated from dissolved Cu concentration at different times, is also represented in Figure 14. This figure shows that, for all the tested configurations, the largest particles (mode 3) represented less than 10 vol % of all particles and a negligible part (less than 2%) of their surface;

moreover, their proportion did not vary significantly during the runs. This is consistent with the data presented in Figure 10, showing that, in the presence of glass beads, the large particles (main mode = $20.1 \mu\text{m}$) contained in the initial pulp are broken during the first hours of stirring.

Right after this short period dominated by particle breakage, the PSD of the particles was rather similar for each type of experiment, with medium particles (mode 2) representing 80–90 vol %, while small particles (mode 1) accounted for about 10 vol %.

Then, the evolution of the PSD depended on the experiment configuration. Indeed, both volume and surface area distributions show that, when leaching was performed with the glass beads, i.e., for the AL and L-AL configurations, contribution of mode 1 increased with time at the expense of mode 2 (Figure 14a,b), indicating the gradual disappearance of medium-sized particles and the production of fine particles. Conversely, the proportions of mode 1 and mode 2 remained rather stable during the A-L experiment, where attrition and leaching were carried out subsequently (Figure 14c). This last observation might indicate that mainly the medium-sized particles were leached, while small particles were made of insoluble phases.

Furthermore, the increase in the population of small particles seems somewhat correlated with leaching rate. Indeed, it is evidenced that the leaching was globally faster in the L-AL configuration than in the AL configuration (especially for $t > 40$

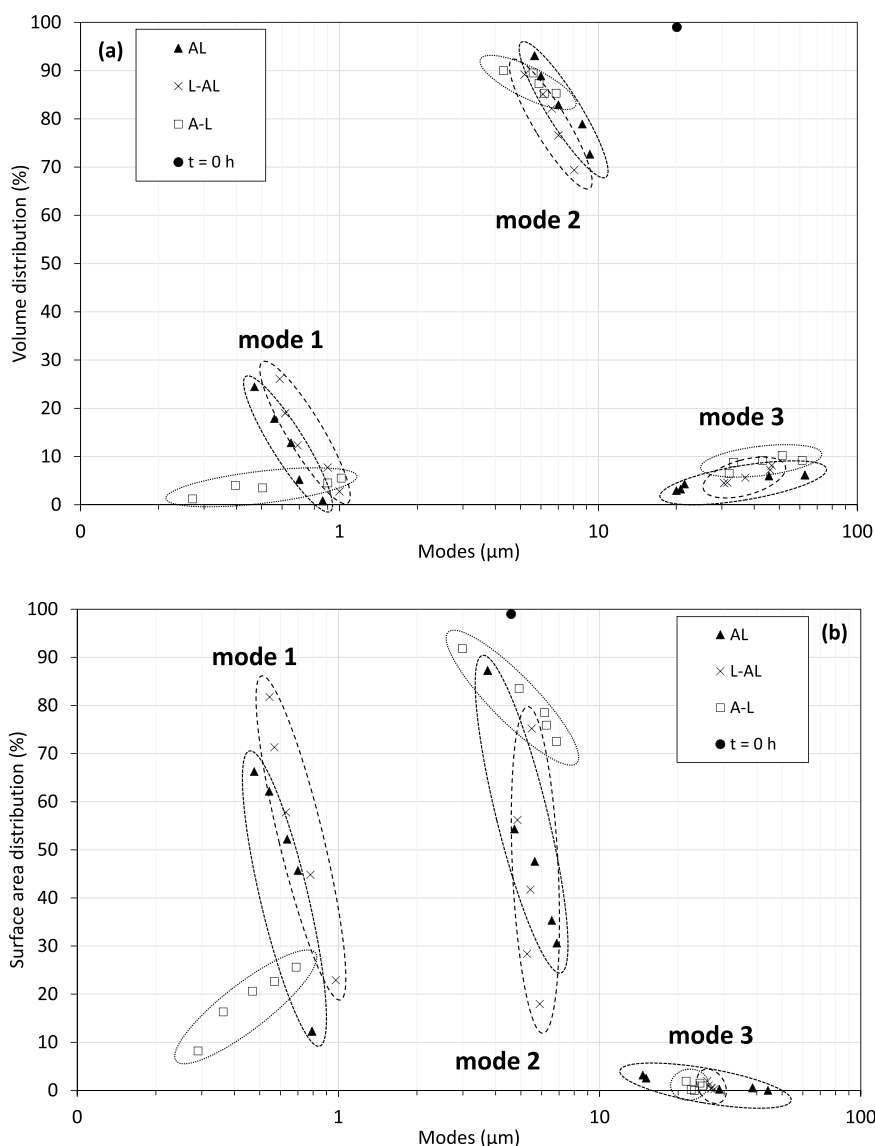


Figure 13. Definition of three major modes from volume (a) and surface area (b) proportions derived from every measured PSD in leaching (L), attrition followed by leaching (A-L), attrition-leaching (AL), and leaching followed by attrition-leaching (L-AL) runs. $t = 0$ corresponds to the reference sample measured in water.

h), and accordingly, the increase in small particles was faster in the former configuration (Figure 14a,b).

4. CONCLUSIONS

In this work, we reported the investigation of a chalcopyrite leaching reactor that implements millimeter-sized grinding glass beads. The article was focused on demonstrating the effect of the attrition phenomenon on the leaching rate and providing a first understanding of the underlying mechanisms. In this objective, we compared the copper leaching yield for different configurations with similar chemical conditions (pH = 1.3, $E_h = 700$ mV vs SHE, and $T = 42$ °C), which brought out the following conclusions:

- Preliminary processing of the chalcopyrite concentrate in a stirred bead reactor for 3 h resulted in an increase of finer particles. As already evidenced in other works, it resulted in an enhancement of the leaching yield thanks to the increase of the initial reactive surface, but the leaching yield remained rather low (<30%) after 120 h.

- Conversely, operating the leaching in the presence of the glass beads provided a remarkable enhancement of the leaching yield (>60% in 48 h), even for particles already passivated by simple leaching.

Regarding the implied chemical reactions, the analyses of the residues showed that, when the leaching was efficient, solid elemental sulfur and jarosite formed, as commonly reported in other works. Moreover, these results are in accordance with the mechanism recently proposed by Ren et al.,²² which envisages the formation of a passivating p–n junction due to a nanoscale layer of covellite. The attrition effect could indeed result in the removal of this thin surface layer, followed by a dissolution of the covellite, which would no longer be inhibited by the p–n junction, to form the usual reaction products.

As for the effect of the glass beads on particle size, we demonstrated that grinding of the particles occurred during a rather short time (~3 h) at the beginning of the runs, shifting the initial PSD with $d_{4/3} = 30$ μm to finer particles with $d_{4/3} = 15$ μm. Based on PSD deconvolution, we showed that particle breakage

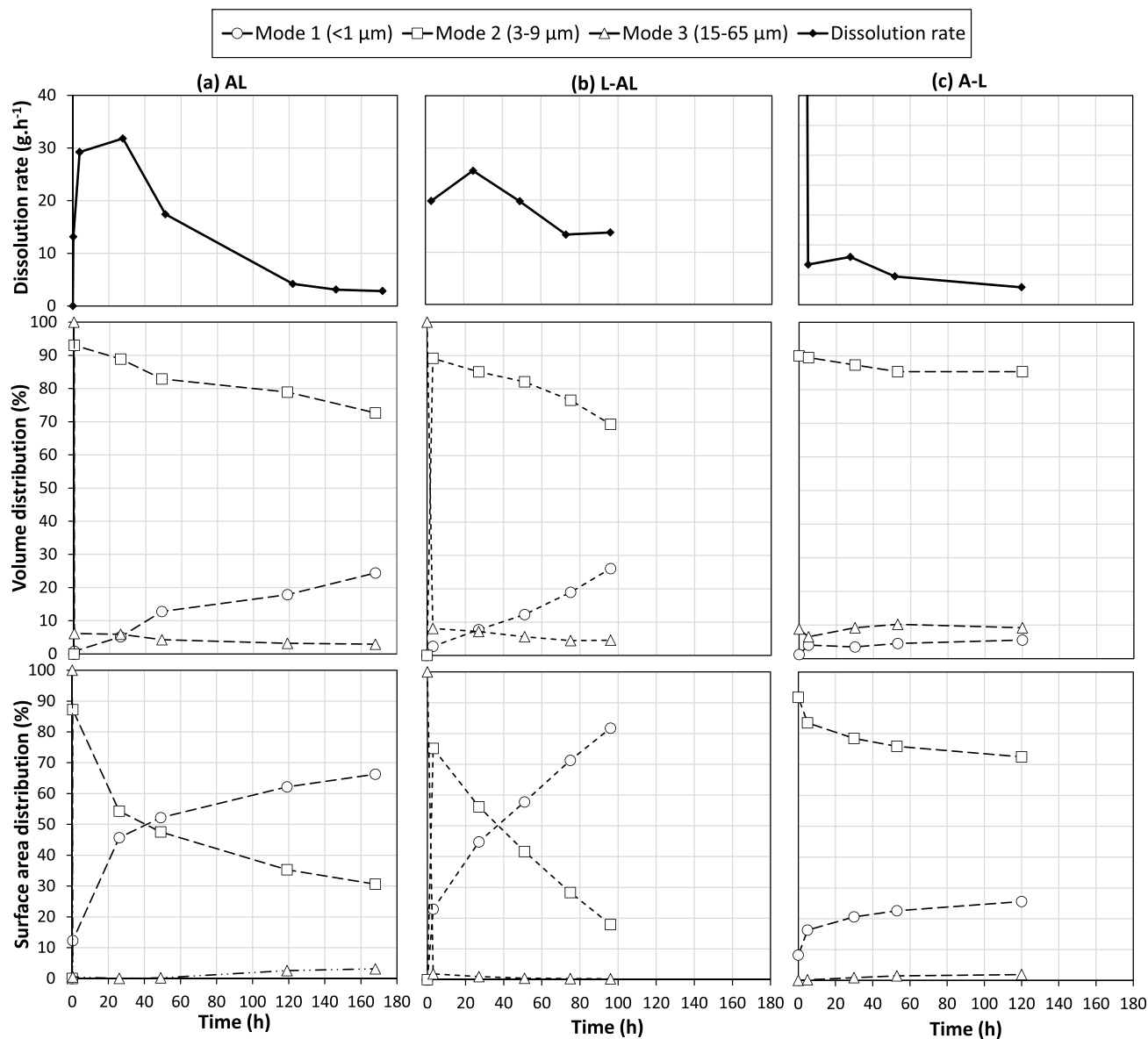


Figure 14. Evolution of dissolution rates and volume and surface area PSDs versus time in (a) attrition-leaching (AL), (b) leaching followed by attrition-leaching (L-AL), and (c) attrition followed by leaching (A-L).

rapidly gave way to the attrition phenomenon, inducing the formation of very fine particles ($<1 \mu\text{m}$) at a rate related to that of copper leaching. Given the aspect of the particles observed by microscopy, agglomeration phenomena of fine particles could also be highlighted. These observations tend to confirm that attrition left a fresh surface of mineral for further leaching. It is also very likely that mechanical activation of the particles contributed to the enhancement of the leaching yield, although quantification of each phenomenon remains a challenge.³⁸

Regarding the possible use of glass beads in an industrial process, many questions remain to be answered. If the reuse of the beads does not seem to be a problem (we recovered more than 99% of the beads after each test), many parameters (e.g., temperature, quantity and hardness of the beads, and amount of concentrate) must be studied and optimized. Also, the additional energy cost required for bead stirring must be quantified. All these elements will allow one to compare the economic and environmental aspects of an attrition-aided

leaching process to other more developed options such as chloride leaching or bioleaching.

AUTHOR INFORMATION

Corresponding Author

Carine Julcour – Laboratoire de Génie Chimique, INP, UPS, Université de Toulouse, CNRS, F-31 432 Toulouse, France; orcid.org/0000-0002-9364-4862; Email: carine.julcour@toulouse-inp.fr

Authors

Amine Dakkoune – Laboratoire de Génie Chimique, INP, UPS, Université de Toulouse, CNRS, F-31 432 Toulouse, France

Florent Bourgeois – Laboratoire de Génie Chimique, INP, UPS, Université de Toulouse, CNRS, F-31 432 Toulouse, France

Adeline Po – Laboratoire de Génie Chimique, INP, UPS, Université de Toulouse, CNRS, F-31 432 Toulouse, France; Water, Environment, Processes & Analyses Division, BRGM

(Bureau de recherches géologiques et minières), F-45100 Orléans, France

Catherine Joulian – Water, Environment, Processes & Analyses Division, BRGM (Bureau de recherches géologiques et minières), F-45100 Orléans, France

Agathe Hubau – Water, Environment, Processes & Analyses Division, BRGM (Bureau de recherches géologiques et minières), F-45100 Orléans, France

Solène Touzé – Water, Environment, Processes & Analyses Division, BRGM (Bureau de recherches géologiques et minières), F-45100 Orléans, France

Anne-Gwénaëlle Guezennec – Water, Environment, Processes & Analyses Division, BRGM (Bureau de recherches géologiques et minières), F-45100 Orléans, France

Laurent Cassayre – Laboratoire de Génie Chimique, INP, UPS, Université de Toulouse, CNRS, F-31 432 Toulouse, France;

© orcid.org/0000-0001-6876-6086

Complete contact information is available at:

<https://pubs.acs.org/10.1021/acseengineeringau.2c00051>

Author Contributions

CRedit: **Amine Dakkoune** data curation (lead), investigation (lead), methodology (equal), writing-original draft (lead); **Florent Bourgeois** conceptualization (equal), formal analysis (equal), methodology (equal), supervision (supporting), writing-original draft (supporting), writing-review & editing (equal); **Adeline Po** investigation (supporting), methodology (supporting), writing-review & editing (supporting); **Catherine Joulian** methodology (supporting), writing-review & editing (supporting); **Agathe Hubau** methodology (supporting), writing-review & editing (supporting); **Solène Touzé** methodology (supporting); **Carine Julcour** conceptualization (equal), methodology (equal), supervision (supporting), writing-original draft (supporting), writing-review & editing (equal); **Anne-Gwénaëlle Guezennec** funding acquisition (supporting), methodology (supporting), supervision (supporting), writing-review & editing (supporting); **Laurent Cassayre** conceptualization (equal), data curation (supporting), funding acquisition (lead), methodology (equal), project administration (lead), supervision (lead), writing-original draft (supporting), writing-review & editing (equal).

Notes

The authors declare no competing financial interest.

ACKNOWLEDGMENTS

This work was funded by the French National Research Agency, project BIOMEALIX under grant no. ANR-18-CE07-0031-01. The supply of chalcopryrite concentrate by Boliden is greatly acknowledged. The authors acknowledge the technical support of Marie-Line De Solan Bethmale and Christine Rey-Rouch for their contribution to the chemical analyses and solid characterizations. The contribution of Jean-Louis Labat, Maiko Ridel, Lahcen Farhi, and Quentin Ribière for the design and assembly of the experimental setup is gratefully acknowledged.

REFERENCES

- Dutrizac, J. E. The kinetics of dissolution of chalcopryrite in ferric ion media. *Metall. Trans. B* **1978**, *9*, 431–439.
- Schlesinger, M.E.; Sole, K.C.; Davenport, W.G.; Alvear Flores, G.R.F. Overview. In *Extr. Metall. Copp*; Sixth Ed.; Schlesinger, M.E., Sole, K.C., Davenport, W.G., Alvear Flores, G.R.F. (Eds.); Elsevier, 2022; pp. 1–18. DOI: [10.1016/B978-0-12-821875-4.00017-1](https://doi.org/10.1016/B978-0-12-821875-4.00017-1).
- Pérez, K.; Toro, N.; Gálvez, E.; Robles, P.; Wilson, R.; Navarra, A. Environmental, economic and technological factors affecting Chilean copper smelters – A critical review. *J. Mater. Res. Technol.* **2021**, *15*, 213–225.
- Klauber, C. A critical review of the surface chemistry of acidic ferric sulphate dissolution of chalcopryrite with regards to hindered dissolution. *Int. J. Miner. Process.* **2008**, *86*, 1–17.
- Li, Y.; Kawashima, N.; Li, J.; Chandra, A. P.; Gerson, A. R. A review of the structure, and fundamental mechanisms and kinetics of the leaching of chalcopryrite. *Adv. Colloid Interface Sci.* **2013**, *197-198*, 1–32.
- Ji, G.; Liao, Y.; Wu, Y.; Xi, J.; Liu, Q. A Review on the Research of Hydrometallurgical Leaching of Low-Grade Complex Chalcopryrite. *J. Sustainable Metall.* **2022**, *8*, 964–977.
- Bogdanović, G. D.; Petrović, S.; Sokić, M.; Antonijević, M. M. Chalcopryrite leaching in acid media: a review. *Metall. Mater. Eng.* **2020**, *26*, 177–198.
- Torres, D.; Ayala, L.; Jeldres, R. I.; Cerecedo-Sáenz, E.; Salinas-Rodríguez, E.; Robles, P.; Toro, N. Leaching Chalcopryrite with High MnO₂ and Chloride Concentrations. *Metals* **2020**, *10*, 107.
- Barton, I. F.; Hiskey, J. B. Chalcopryrite leaching in novel lixiviants. *Hydrometallurgy* **2022**, *207*, No. 105775.
- Vera Véliz, M.; Videla Leiva, A.; Martínez Bellange, P., Copper Bioleaching Operations in Chile: Towards New Challenges and Developments. In *Bioleaching Technol. Extr. Recover. Met*; Johnson, D.B., Bryan, C.G., Schlömann, M., Roberto, F.F. (Eds.), Ores Wastes, Springer International Publishing, Cham, 2023; pp. 163–176 DOI: [10.1007/978-3-031-05382-5_9](https://doi.org/10.1007/978-3-031-05382-5_9).
- Roberto, F. F.; Schippers, A. Progress in bioleaching: part B, applications of microbial processes by the minerals industries. *Appl. Microbiol. Biotechnol.* **2022**, *106*, 5913–5928.
- Debernardi, G.; Carlesi, C. Chemical-Electrochemical Approaches to the Study Passivation of Chalcopryrite Miner. Process. *Extr. Metall. Rev.* **2013**, *34*, 10–41.
- Córdoba, E. M.; Muñoz, J. A.; Blázquez, M. L.; González, F.; Ballester, A. Leaching of chalcopryrite with ferric ion Part I: General aspects. *Hydrometallurgy* **2008**, *93*, 81–87.
- Khoshkhou, M.; Dopson, M.; Engström, F.; Sandström, Å. New insights into the influence of redox potential on chalcopryrite leaching behaviour. *Miner. Eng.* **2017**, *100*, 9–16.
- Hackl, R. P.; Dreisinger, D. B.; Peters, E.; King, J. A. Passivation of chalcopryrite during oxidative leaching in sulfate media. *Hydrometallurgy* **1995**, *39*, 25–48.
- McMillan, R. S.; MacKinnon, D. J.; Dutrizac, J. E. Anodic dissolution of n-type and p-type chalcopryrite. *J. Appl. Electrochem.* **1982**, *12*, 743–757.
- Sasaki, K.; Nakamura, Y.; Hirajima, T.; Tuovinen, O. H. Raman characterization of secondary minerals formed during chalcopryrite leaching with *Acidithiobacillus ferrooxidans*. *Hydrometallurgy* **2009**, *95*, 153–158.
- Parker, A.; Klauber, C.; Kougiannos, A.; Watling, H. R.; van Bronswijk, W. An X-ray photoelectron spectroscopy study of the mechanism of oxidative dissolution of chalcopryrite. *Hydrometallurgy* **2003**, *71*, 265–276.
- Sandström, Å.; Shchukarev, A.; Paul, J. XPS characterisation of chalcopryrite chemically and bio-leached at high and low redox potential. *Miner. Eng.* **2005**, *18*, 505–515.
- Zhu, W.; Xia, J.; Yang, Y.; Nie, Z.; Zheng, L.; Ma, C.; Zhang, R.; Peng, A.; Tang, L.; Qiu, G. Sulfur oxidation activities of pure and mixed thermophiles and sulfur speciation in bioleaching of chalcopryrite. *Bioresour. Technol.* **2011**, *102*, 3877–3882.
- O'Connor, G. M.; Eksteen, J. J. A critical review of the passivation and semiconductor mechanisms of chalcopryrite leaching. *Miner. Eng.* **2020**, *154*, No. 106401.
- Ren, Z.; Chao, C.; Krishnamoorthy, P.; Asselin, E.; Dixon, D. G.; Mora, N. The overlooked mechanism of chalcopryrite passivation. *Acta Mater.* **2022**, *236*, No. 118111.
- Watling, H. R. Chalcopryrite hydrometallurgy at atmospheric pressure: 1. Review of acidic sulfate, sulfate–chloride and sulfate–nitrate process options. *Hydrometallurgy* **2013**, *140*, 163–180.

- (24) McDonald, R. G.; Muir, D. M. Pressure oxidation leaching of chalcopyrite. Part I. Comparison of high and low temperature reaction kinetics and products. *Hydrometallurgy* **2007**, *86*, 191–205.
- (25) Baláz, P., Mechanochemistry in Minerals Engineering. In *Mechanochemistry Nanosci. Miner Eng*; Springer: Berlin, Heidelberg, 2008; pp. 257–296, DOI: 10.1007/978-3-540-74855-7_5.
- (26) Granata, G.; Takahashi, K.; Kato, T.; Tokoro, C. Mechanochemical activation of chalcopyrite: Relationship between activation mechanism and leaching enhancement. *Miner. Eng.* **2019**, *131*, 280–285.
- (27) Khezri, M.; Rezai, B.; Abdollahzadeh, A. A.; Wilson, B. P.; Molaieinasab, M.; Lundström, M. Investigation into the effect of mechanical activation on the leaching of chalcopyrite in a glycine medium. *Hydrometallurgy* **2021**, *203*, No. 105492.
- (28) Tesinsky, M., Balaz, P., *Copper Leaching from Chalcopyrite: Mechanochemical Approach*, *Inż. Miner. R.* **18**, nr 1 (2017). <http://yadda.icm.edu.pl/baztech/element/bwmeta1.element/baztech-7c778661-d073-4fd0-a6ba-aa659d577614> (accessed October 14, 2021).
- (29) Yang, H.; Zhao, S.; Wang, G.; Zhang, Q.; Jin, Z.; Tong, L.; Chen, G.; Qiu, X. Mechanical activation modes of chalcopyrite concentrate and relationship between microstructure and leaching efficiency. *Hydrometallurgy* **2022**, *207*, No. 105778.
- (30) Bai, Y.; Wang, W.; Zhao, S.; Lu, D.; Xie, F.; Dreisinger, D. Effect of Mechanical Activation on Leaching Behavior and Mechanism of Chalcopyrite Miner. Process. *Extr. Metall. Rev.* **2022**, *43*, 440–452.
- (31) Li, Y.; Yao, Y.; Wang, B.; Qian, G.; Li, Z.; Zhu, Y. New insights into chalcopyrite leaching enhanced by mechanical activation. *Hydrometallurgy* **2019**, *189*, No. 105131.
- (32) Misra, M.; Fuerstenau, M. C. Chalcopyrite leaching at moderate temperature and ambient pressure in the presence of nanosize silica. *Miner. Eng.* **2005**, *18*, 293–297.
- (33) Dong, Y. B.; Lin, H.; Zhou, S.; Xu, X.; Zhang, Y. Effects of quartz addition on chalcopyrite bioleaching in shaking flasks. *Miner. Eng.* **2013**, *46–47*, 177–179.
- (34) Jafari, M.; Karimi, G.; Ahmadi, R. Improvement of chalcopyrite atmospheric leaching using controlled slurry potential and additive treatments. *Physicochem. Probl. Miner. Process.* **2017**, *53*, 53.
- (35) Bodénan, F.; Bourgeois, F.; Petiot, C.; Augé, T.; Bonfils, B.; Julcour-Lebigue, C.; Guyot, F.; Boukary, A.; Tremosa, J.; Lassin, A.; Gaucher, E. C.; Chiquet, P. Ex situ mineral carbonation for CO₂ mitigation: Evaluation of mining waste resources, aqueous carbonation processability and life cycle assessment (Carmex project). *Miner. Eng.* **2014**, *59*, 52–63.
- (36) Bonfils, B.; Julcour-Lebigue, C.; Guyot, F.; Bodénan, F.; Chiquet, P.; Bourgeois, F. Comprehensive analysis of direct aqueous mineral carbonation using dissolution enhancing organic additives. *Int. J. Greenh. Gas Control.* **2012**, *9*, 334–346.
- (37) Julcour, C.; Bourgeois, F.; Bonfils, B.; Benhamed, I.; Guyot, F.; Bodénan, F.; Petiot, C.; Gaucher, E. C. Development of an attrition-leaching hybrid process for direct aqueous mineral carbonation. *Chem. Eng. J.* **2015**, *262*, 716–726.
- (38) Rim, G.; Wang, D.; Rayson, M.; Brent, G.; Park, A.-H. A. Investigation on Abrasion versus Fragmentation of the Si-rich Passivation Layer for Enhanced Carbon Mineralization via CO₂ Partial Pressure Swing. *Ind. Eng. Chem. Res.* **2020**, *59*, 6517–6531.
- (39) Julcour, C.; Cassayre, L.; Benhamed, I.; Diouani, J.; Bourgeois, F. Insights Into Nickel Slag Carbonation in a Stirred Bead Mill. *Front. Chem. Eng.* **2020**, *2*, 21.
- (40) Mulligan, M.; Chaiko, D.; Baczek, F.; Rocks, S.; Eyzaguirre, C.; Dickinson, C.; Klepper, R. The FLSmidth® Rapid Oxidative Leach (ROL) process: a mechano-chemical approach and industrial applications for rapid metal sulphide dissolution. *J. South. Afr. Inst. Min. Metall.* **2017**, *117*, 741–747.
- (41) Senanayake, G., Miki, H. S. *Wheatley, Silica and sodium chloride assisted leaching of chalcopyrite* Canadian Institute of Mining, Metallurgy & Petroleum; *I*, 2014; pp. 211–223.
- (42) Garrels, R.M., Christ, C.L., *Solution, Minerals, and Equilibria*, Harper Row; Cambridge University Press, 1965 213–233.
- (43) Guezennec, A.-G., d'Hugues, P., Bioprocessing low grade copper ores - a promising alternative In *13th SGA Bienn. Meet.*, Georesources Nancy, France, 2015. <https://hal-brgm.archives-ouvertes.fr/hal-01154886> (accessed September 30, 2021).
- (44) Nicol, M. J. The role and use of hydrogen peroxide as an oxidant in the leaching of minerals. 1. acid solutions. *Hydrometallurgy* **2020**, *193*, No. 105328.
- (45) Scholz, F., ed., *Electroanalytical Methods: Guide to Experiments and Applications*; 2nd ed., Springer-Verlag: Berlin Heidelberg, 2010 DOI: 10.1007/978-3-642-02915-8.
- (46) Dreisinger, D.; Abed, N. A fundamental study of the reductive leaching of chalcopyrite using metallic iron part I: kinetic analysis. *Hydrometallurgy* **2002**, *66*, 37–57.
- (47) Tanne, C.; Schippers, A. Electrochemical investigation of microbially and galvanically leached chalcopyrite. *Hydrometallurgy* **2021**, *202*, No. 105603.
- (48) Dixon, D. G.; Mayne, D. D.; Baxter, K. G. Galvanox™ – a Novel Galvanically-Assisted Atmospheric Leaching Technology for Copper Concentrates. *Can. Metall. Q.* **2008**, *47*, 327–336.
- (49) Nicol, M. J. Does galvanic coupling with pyrite increase the rate of dissolution of chalcopyrite under ambient conditions? An electrochemical study. *Hydrometallurgy* **2022**, *208*, No. 105824.
- (50) Li, Y.; Qian, G.; Li, J.; Gerson, A. R. Kinetics and roles of solution and surface species of chalcopyrite dissolution at 650mV. *Geochim. Cosmochim. Acta* **2015**, *161*, 188–202.
- (51) Li, Y.; Wei, Z.; Qian, G.; Li, J.; Gerson, A. R. Kinetics and Mechanisms of Chalcopyrite Dissolution at Controlled Redox Potential of 750 mV in Sulfuric Acid Solution. *Minerals* **2016**, *6*, 83.
- (52) Ma, Y.; Lin, C. Microbial Oxidation of Fe²⁺ and Pyrite Exposed to Flux of Micromolar H₂O₂ in Acidic Media. *Sci. Rep.* **2013**, *3*, 1979.
- (53) Hubau, A.; Guezennec, A.-G.; Joulian, C.; Falagán, C.; Dew, D.; Hudson-Edwards, K. A. Bioleaching to reprocess sulfidic polymetallic primary mining residues: Determination of metal leaching mechanisms. *Hydrometallurgy* **2020**, *197*, No. 105484.
- (54) Dufourny, A.; Julcour, C.; Esvan, J.; Cassayre, L.; Laniésse, P.; Bourgeois, F. Observation of the depassivation effect of attrition on magnesium silicates' direct aqueous carbonation products. *Front. Clim.* **2022**, *4*, 139. (accessed August 23, 2022)